

# Performance Enhancement of $\text{Ga}_2\text{O}_3$ Solar-Blind UV Photodetector by the Combination of Oxygen Annealing and Plasma Treatment

Chao Zhang, Kewei Liu,\* Qiu Ai, Xiaoqian Huang, Xing Chen, Yongxue Zhu, Jialin Yang, Zhen Cheng, Binghui Li, Lei Liu, and Dezhen Shen\*



Cite This: *J. Phys. Chem. C* 2022, 126, 21839–21846



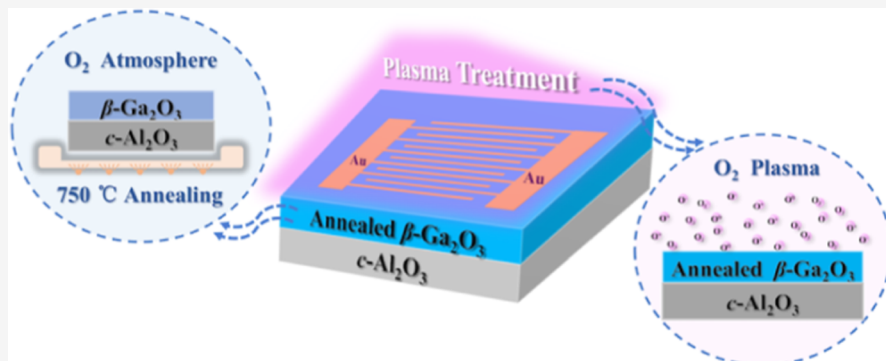
Read Online

ACCESS |

Metrics & More

Article Recommendations

Supporting Information



**ABSTRACT:** Monoclinic  $\text{Ga}_2\text{O}_3$  ( $\beta\text{-}\text{Ga}_2\text{O}_3$ ) meets the demand of intrinsic solar-blind photodetection for various applications. Currently, it is still very challenging to realize excellent  $\beta\text{-}\text{Ga}_2\text{O}_3$  solar-blind photodetectors. Here, we demonstrated a high-performance solar-blind ultraviolet (UV) photodetector based on  $\beta\text{-}\text{Ga}_2\text{O}_3$  thin films by combining high-temperature oxygen annealing and oxygen plasma treatment. A high normalized photo-to-dark current ratio of  $1.3 \times 10^{12} \text{ W}^{-1}$ , a large rejection ratio ( $R_{\text{peak}}/R_{400}$ ) of  $8.6 \times 10^6$ , and fast rise/decay times of 0.6/0.5 s have been obtained from the annealed & plasma-treated  $\beta\text{-}\text{Ga}_2\text{O}_3$  photodetector. Moreover, the effects of the combination of oxygen annealing and oxygen plasma treatment on the properties of  $\beta\text{-}\text{Ga}_2\text{O}_3$  films and their photodetectors were investigated. The results indicated that the improved solar-blind photodetection performance can be attributed to the reduction of the oxygen vacancy defects and the modification of the surface states of the  $\text{Ga}_2\text{O}_3$  films after oxygen annealing and plasma treatment in sequence. Our findings in this work provides a potential way to improve the performance of  $\text{Ga}_2\text{O}_3$  film-based solar-blind UV photodetectors.

## 1. INTRODUCTION

Solar-blind ultraviolet (UV) photodetectors have recently received widespread attention due to their important applications in environment monitoring, flame detection, missile warning, space communication, and so on.<sup>1–4</sup> Currently, the solar-blind UV photodetectors based on wide-band gap semiconductor materials including AlGaN, ZnMgO, diamond, and  $\text{Ga}_2\text{O}_3$  have been recognized as emerging UV detectors.<sup>5–8</sup> Among these wide-band gap semiconductors,  $\text{Ga}_2\text{O}_3$  is considered as one of the most ideal materials for solar-blind UV photodetection due to its suitable direct band gap of  $\sim 4.7\text{--}5.2$  eV, high radiation hardness, and high stability.<sup>9–12</sup> In particular, monoclinic  $\text{Ga}_2\text{O}_3$  ( $\beta\text{-}\text{Ga}_2\text{O}_3$ ), as the most stable phase of  $\text{Ga}_2\text{O}_3$ , has been extremely investigated in the past few years for the fabrication of solar-blind UV photodetectors.<sup>13–16</sup> To date, large numbers of  $\beta\text{-}\text{Ga}_2\text{O}_3$  photodetectors have been demonstrated based on different structures, such as metal–semiconductor–metal (MSM) structure, Schottky junctions, heterojunctions, and

so on. These reported  $\beta\text{-}\text{Ga}_2\text{O}_3$  devices commonly exhibit high responsivity.<sup>17–20</sup> Nevertheless, the dark current and UV-visible rejection ratio of  $\beta\text{-}\text{Ga}_2\text{O}_3$  solar-blind UV photodetectors are significantly worse than expected due to the existence of large amounts of oxygen vacancy defects.<sup>21–24</sup> To eliminate the influence of oxygen vacancy defects on the device performance, high-temperature annealing under oxygen atmosphere has been regarded as an effective technology, which can not only reduce the number of defects but also improve the crystal quality. So far, numerous reports are available on the effect of oxygen annealing on the properties of  $\text{Ga}_2\text{O}_3$  films and their photodetectors.<sup>25–27</sup> Rafique et al. have

Received: October 11, 2022

Revised: December 5, 2022

Published: December 19, 2022



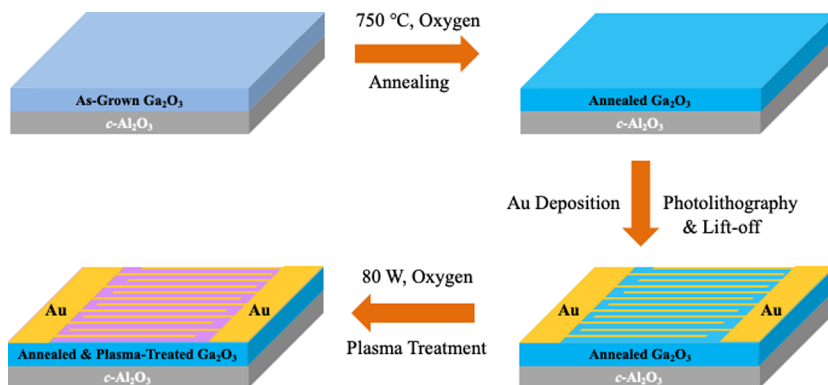


**Figure 1.** Schematic illustration of the fabrication processes of  $\beta$ - $\text{Ga}_2\text{O}_3$  MSM photodetectors.

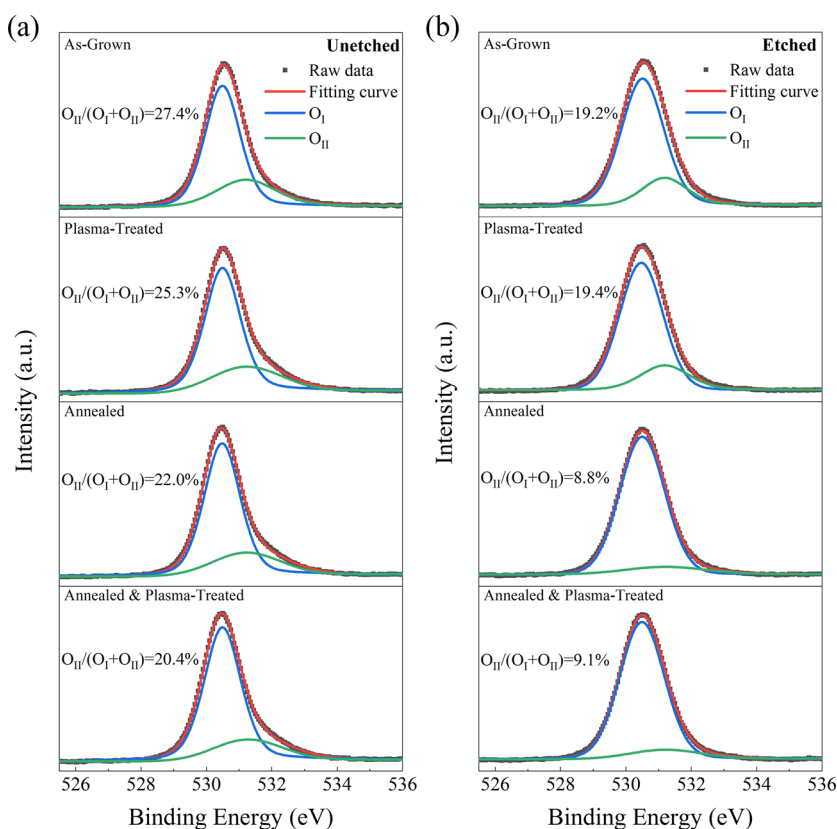


**Figure 2.** O 1s XPS spectra of the  $\beta$ - $\text{Ga}_2\text{O}_3$  films before (a) and after (b) Ar ion etching.

demonstrated a significant suppression of the dark current and a large enhancement in the out of band rejection ratio in  $\beta$ - $\text{Ga}_2\text{O}_3$  solar-blind photodetector by annealing the  $\beta$ - $\text{Ga}_2\text{O}_3$  thin film in oxygen atmosphere at 1000 °C.<sup>27</sup> Our previous study showed that oxygen annealing could improve the response speed and UV-visible rejection ratio, obviously, of the amorphous  $\text{Ga}_2\text{O}_3$  solar-blind photodetector.<sup>24</sup> However, although high-temperature oxygen annealing can repair oxygen vacancy defects inside  $\text{Ga}_2\text{O}_3$  and improve the crystalline quality, it has no obvious effect on surface states that often cause photogenerated carrier recombination and increase the leakage current. In contrast, plasma treatment has been commonly regarded as a good method to tailor the surface characteristics of different semiconductor materials, such as ZnO, GaN, and so on.<sup>28–30</sup> However, plasma treatment mainly affects the surface and cannot repair the defects inside the materials. Therefore, the combination of high-temperature

oxygen annealing and oxygen plasma treatment on the  $\text{Ga}_2\text{O}_3$  film is expected to efficiently improve the crystalline quality, repair the internal and surface oxygen vacancy defects, and modify the surface states. So far, no studies have focused on the effect of the combination of annealing and plasma treatment on the performance of the  $\text{Ga}_2\text{O}_3$ -based photodetectors.

In this work, the MSM solar-blind UV photodetectors were demonstrated on  $\beta$ - $\text{Ga}_2\text{O}_3$  thin films by metal–organic chemical vapor deposition (MOCVD). The effect of the combination of high-temperature oxygen annealing and subsequent oxygen plasma treatment on the crystalline quality and optical and photoresponse properties of  $\beta$ - $\text{Ga}_2\text{O}_3$  thin films was systematically investigated. Compared to the as-grown, plasma-treated-only, and annealed-only devices, the annealed & plasma-treated  $\beta$ - $\text{Ga}_2\text{O}_3$  photodetector exhibits

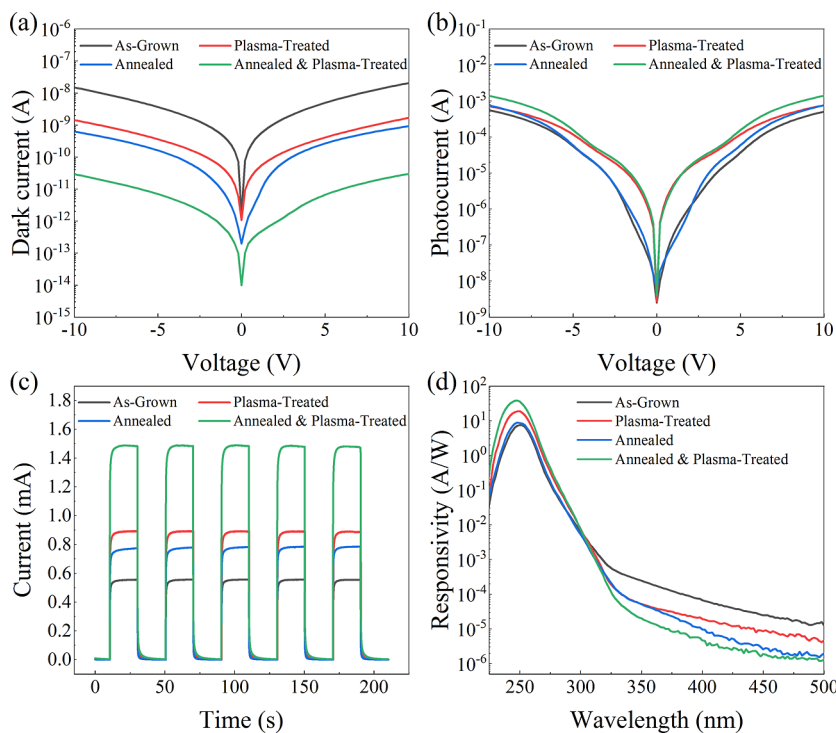


**Figure 3.** Semilogarithmic  $I$ – $V$  characteristics of the  $\beta$ - $\text{Ga}_2\text{O}_3$  MSM photodetectors (a) in the dark and (b) under 254 nm illumination. (c) Time-dependent photoresponse with the 254 nm light periodically on and off at 10 V. (d) Spectral response on a semilogarithmic scale at 10 V.

superior performance. The detailed mechanism for the above phenomenon was also discussed.

## 2. EXPERIMENTAL SECTION

The  $\beta$ - $\text{Ga}_2\text{O}_3$  thin films were grown on  $c$ - $\text{Al}_2\text{O}_3$  substrates by MOCVD. The growth temperature was kept at 700 °C with a chamber pressure of  $1.7 \times 10^3$  Pa. Triethylgallium (TEGa) and high-purity oxygen were used as precursors, and the carrier gas was high-purity nitrogen. The flow rates of TEGa and oxygen were set at 4 and 120 sccm, respectively. After the growth, high-temperature annealing was carried out in a horizontal tube furnace under pure oxygen atmosphere (standard atmospheric pressure of  $\sim 1 \times 10^5$  Pa) for 40 min at a temperature of 750 °C. The  $\beta$ - $\text{Ga}_2\text{O}_3$  MSM photodetectors with Au interdigital electrodes (40 nm thick) were fabricated using photolithography and lift-off techniques. The Au fingers are 10  $\mu\text{m}$  wide and 500 nm long with 10  $\mu\text{m}$  spacing. After that, the devices were exposed to oxygen plasma with a power of 80 W for 10 min, which was produced through a radio-frequency plasma source. Figure 1 shows the schematic illustration of the fabrication processes of  $\beta$ - $\text{Ga}_2\text{O}_3$  MSM photodetectors.

The morphology and structural property of  $\beta$ - $\text{Ga}_2\text{O}_3$  films were characterized by scanning electron microscopy (SEM) (Hitachi S-4800) and X-ray diffractometer (XRD) (Cu K $\alpha$  radiation,  $\lambda = 0.154$  nm). The elemental composition and chemical state were investigated by X-ray photoelectron spectroscopy (XPS). Transmission spectra were recorded using a Shimadzu UV-3101PC spectrophotometer. The current–voltage ( $I$ – $V$ ) properties and time-dependent photocurrent ( $I$ – $t$ ) curves were measured by a semiconductor parameter analyzer (Agilent B1500A). The response spectra were obtained by using a 200 W UV enhanced Xe lamp and a monochromator.

## 3. RESULTS AND DISCUSSION

The morphology, thickness, and structural and optical properties of as-grown, oxygen plasma-treated, 750 °C oxygen-annealed, and annealed & plasma-treated  $\beta$ - $\text{Ga}_2\text{O}_3$  films were characterized by SEM, XRD, and UV–visible transmission spectra as shown in Figure S1. Obviously, all  $\beta$ - $\text{Ga}_2\text{O}_3$  films have a uniform granular surface morphology with a thickness of approximately 170 nm. In addition, all films show a high transmittance of over 90% in the visible region with sharp absorption edges at  $\sim 250$  nm. The band gaps of  $\beta$ - $\text{Ga}_2\text{O}_3$  films are estimated to be  $\sim 4.94$  eV, which is close to the most reported values.<sup>31</sup> Moreover,  $\beta$ - $\text{Ga}_2\text{O}_3$  thin films fabricated on the  $c$ -face sapphire substrate have a (201) preferred orientation, and the full width at half-maximum of (201) peak is  $\sim 0.2^\circ$  for all samples. The SEM, XRD, and optical transmission spectra results indicate that no obvious changes in the surface morphology, thickness, crystalline quality, and optical property of the  $\beta$ - $\text{Ga}_2\text{O}_3$  thin films can be observed before and after oxygen annealing and/or oxygen plasma treatment in our case.

To further investigate the chemical state of the  $\beta$ - $\text{Ga}_2\text{O}_3$  films before and after oxygen annealing and/or oxygen plasma treatment, XPS measurement combined with argon gas cluster etching have been conducted. Figure 2a,b shows the O 1s XPS spectra of  $\beta$ - $\text{Ga}_2\text{O}_3$  films before and after etching, respectively. Each O 1s XPS spectrum can be divided into two components: an intense peak ( $\text{O}_{\text{I}}$ ) is located at about 530.5 eV, which is related to the Ga–O bond of  $\text{Ga}_2\text{O}_3$ , while the other one ( $\text{O}_{\text{II}}$ ) is observed at about 531.2 eV corresponding to the  $\text{O}^{2-}$  ions in the oxygen-deficient regions.<sup>32–34</sup> The integrated peak area intensity ratios of  $\text{O}_{\text{II}}/(\text{O}_{\text{I}} + \text{O}_{\text{II}})$  can be used to determine the densities of oxygen vacancy defects. Obviously, the content of surface oxygen vacancy defects (before etching) is higher than that of bulk oxygen vacancy defects (after etching) for all  $\beta$ -

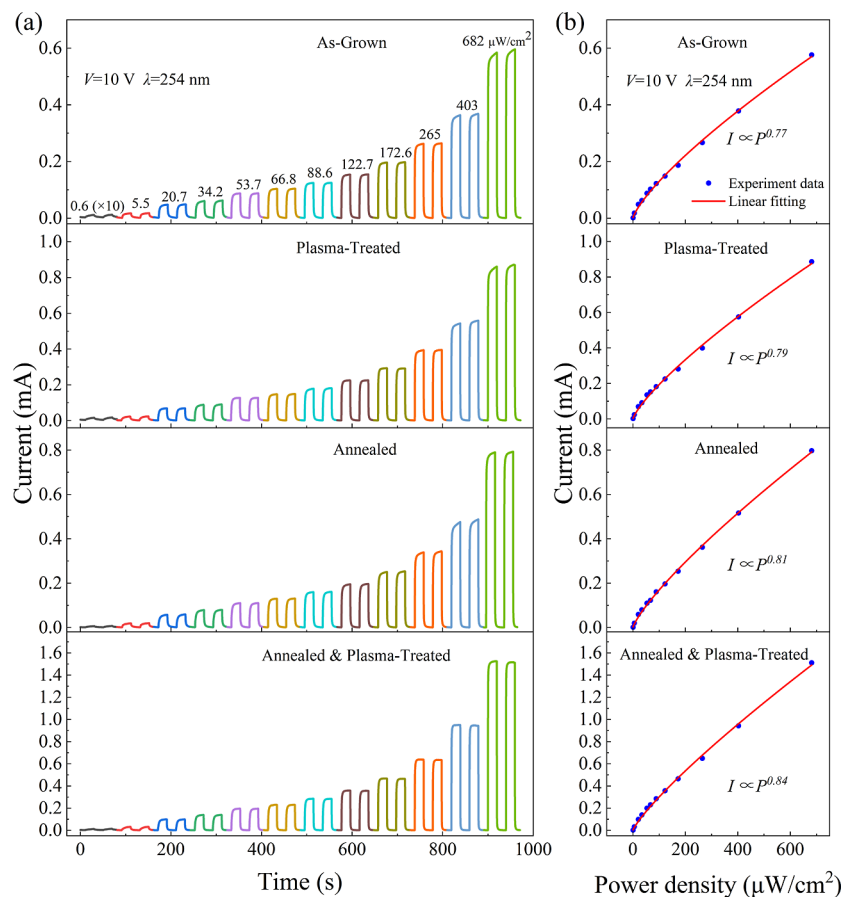


**Figure 4.** (a) Time-dependent photoresponse under 254 nm illumination with different intensities biased at 10 V. (b) Photocurrent as a function of illumination intensity at 10 V.

$\text{Ga}_2\text{O}_3$  films. Figure 2a shows the XPS spectra of  $\text{Ga}_2\text{O}_3$  films without etching. It can be found that the  $\text{O}_{\text{II}}/(\text{O}_1 + \text{O}_{\text{II}})$  ratios at the surface of the as-grown, oxygen plasma-treated, high-temperature oxygen annealed, and annealed & plasma-treated films are  $\sim 27.4$ ,  $\sim 25.3$ ,  $\sim 22.0$ , and  $\sim 20.4\%$ , respectively. Figure 2b displays the XPS depth-profile analysis with the etching rate of 0.25 nm/s for 160 s. Obviously, the  $\text{O}_{\text{II}}/(\text{O}_1 + \text{O}_{\text{II}})$  ratios inside  $\beta\text{-Ga}_2\text{O}_3$  films are  $\sim 19.2$ ,  $\sim 19.4$ ,  $\sim 8.8$ , and  $\sim 9.1\%$  for the as-grown, plasma-treated, annealed, and annealed & plasma-treated samples, respectively. The XPS results indicate that high-temperature oxygen annealing can significantly reduce the oxygen vacancy defects inside  $\text{Ga}_2\text{O}_3$  films and also have a certain repair effect on the surface oxygen vacancy defects. In contrast, oxygen plasma treatment can only slightly reduce the oxygen vacancy defects on the surface of  $\text{Ga}_2\text{O}_3$  films but almost has no effect on the oxygen vacancy defects inside the films.

Figure 3a,b gives the semilogarithmic  $I-V$  characteristics of the  $\beta\text{-Ga}_2\text{O}_3$  photodetectors in the dark and under 254 nm illumination (power density  $\sim 0.7$  mW/cm $^2$ ) at room temperature, respectively. As shown in Figure 3a, the dark currents of both the annealed and plasma-treated  $\beta\text{-Ga}_2\text{O}_3$  MSM photodetectors were obviously less than that of the as-grown device by about 1 order of magnitude. More interestingly, by combining high-temperature oxygen annealing and oxygen plasma treatment, the dark current of  $\beta\text{-Ga}_2\text{O}_3$  MSM photodetector is further significantly reduced to  $\sim 29$  pA at 10 V, which is nearly 3 orders of magnitude lower than that of the as-grown device ( $\sim 21$  nA at 10 V). The decrease in the

dark current of the devices can be attributed to the elimination of surface leakage channels by plasma treatment and the reduction of the oxygen-related defects by annealing. At the same time, the effects of different atmospheres and treatment time of plasma treatment on the dark current were also investigated (as shown in Figure S2). Additionally, it can be clearly obtained that the photocurrent of the photodetectors increased slightly by oxygen annealing and/or plasma treatment, and the reduction of defect-related recombination of photogenerated carriers should be the main reason for this trend. Therefore, benefiting from the reduction of dark current and the enhancement of photocurrent, the normalized photo-to-dark current ratio (NPDR) of the annealed & plasma-treated  $\beta\text{-Ga}_2\text{O}_3$  film photodetector is as high as  $1.3 \times 10^{12}$  W $^{-1}$  under 250 nm illumination at 10 V, which is nearly 10,000 times higher than that of the device based on as-grown  $\beta\text{-Ga}_2\text{O}_3$  film.

The time-dependent photoresponse characteristics of the  $\beta\text{-Ga}_2\text{O}_3$  photodetectors were investigated with the 254 nm light periodically on and off at 10 V bias as illustrated in Figure 3c. All devices demonstrate good repeatability and stability. Moreover, the 10–90% rise time and 90–10% decay time of the devices have been estimated to be  $\sim 0.6$  and  $\sim 0.5$  s from a single cycle of photoresponse curve, respectively.

Figure 3d shows the spectral responses on a semilogarithmic scale at 10 V bias. The spectral response peaks of all four devices appear near 250 nm with a  $-3$  dB cutoff at  $\sim 260$  nm. The UV to visible rejection ratio ( $R_{\text{peak}}/R_{400}$ ) is defined as the ratio between the peak responsivity and responsivity at 400

**Table 1.** Performance Parameters of the  $\beta$ -Ga<sub>2</sub>O<sub>3</sub> Photodetectors at 10 V in This Work

device	dark current (nA)	responsivity (A W <sup>-1</sup> )	rejection ratio ( $R_{\text{peak}}/R_{400}$ )	NPDR (W <sup>-1</sup> )	detectivity (cm Hz <sup>1/2</sup> W <sup>-1</sup> )
as-grown	21	7.54	$1.1 \times 10^4$	$3.6 \times 10^8$	$6.5 \times 10^{13}$
plasma-treated	1.7	18.96	$9.9 \times 10^5$	$1.1 \times 10^{10}$	$5.7 \times 10^{14}$
annealed	0.92	8.85	$9.1 \times 10^5$	$9.6 \times 10^9$	$3.6 \times 10^{14}$
annealed & plasma-treated	$2.9 \times 10^{-2}$	38.82	$8.6 \times 10^6$	$1.3 \times 10^{12}$	$9.0 \times 10^{15}$

**Table 2.** Comparison of Devices Performance of Our Annealed & Plasma-Treated Device and Other MSM Photodetectors Based on Ga<sub>2</sub>O<sub>3</sub> Thin Films

materials	method	dark current (nA)	responsivity (A W <sup>-1</sup> )	rejection ratio	detectivity (cm Hz <sup>1/2</sup> W <sup>-1</sup> )	refs
$\alpha$ -Ga <sub>2</sub> O <sub>3</sub>	LMBE	1.02@10 V	0.0151@20 V			38
$\alpha$ -Ga <sub>2</sub> O <sub>3</sub>	ALD	$5 \times 10^{-4}$ @10 V	0.76@20 V	$3.57 \times 10^2 (R_{253}/R_{400})$		39
$\epsilon$ -Ga <sub>2</sub> O <sub>3</sub>	MOCVD	$2.5 \times 10^{-2}$ @6 V	84@6 V		$4.2 \times 10^{14}$	40
$\alpha$ -Ga <sub>2</sub> O <sub>3</sub>	magnetron sputtering	0.3386@10 V	76.26@10 V	$1.15 \times 10^5 (R_{250}/R_{350})$	$1.26 \times 10^{14}$	33
$\alpha$ -Ga <sub>2</sub> O <sub>3</sub>	magnetron sputtering	$1.63 \times 10^4$ @5 V	55.5@5 V	$10^3$	$1.14 \times 10^{12}$	36
$\alpha$ -Ga <sub>2</sub> O <sub>3</sub>	ALD	$9.43 \times 10^{-3}$ @10 V	1.34@10 V	$2.74 \times 10^5 (R_{250}/R_{400})$		24
$\beta$ -Ga <sub>2</sub> O <sub>3</sub>	LMBE		0.21@8 V	$>10^3$		41
$\beta$ -Ga <sub>2</sub> O <sub>3</sub>	MOCVD		46@20 V	$10^7 (R_{250}/R_{365})$	$9.8 \times 10^{15}$	42
$\beta$ -Ga <sub>2</sub> O <sub>3</sub>	PLD	$4 \times 10^{-2}$ @10 V	0.35@10 V			43
$\beta$ -Ga <sub>2</sub> O <sub>3</sub>	PLD	$1.2 \times 10^{-2}$ @5 V	0.903@5 V	$7.867 \times 10^3 (R_{250}/R_{350})$		44
$\beta$ -Ga <sub>2</sub> O <sub>3</sub>	MBE	4@20 V	$>1.5 @ 4$ V	$>10^5 (R_{236}/R_{420})$		9
$\beta$ -Ga <sub>2</sub> O <sub>3</sub>	LMBE	1.9@10 V	0.06@10 V			45
$\beta$ -Ga <sub>2</sub> O <sub>3</sub>	PA-MBE	1.9@20 V	170.2@20 V		$1.3 \times 10^{14}$	46
$\beta$ -Ga <sub>2</sub> O <sub>3</sub>	MOCVD	$2.9 \times 10^{-2}$ @10 V	38.82@10 V	$8.6 \times 10^6 (R_{250}/R_{400})$	$9.0 \times 10^{15}$	this work

nm, which can be used to evaluate the spectral selectivity of the photodetector. As we can see, the UV-visible rejection ratio of the photodetectors can be improved from  $1.1 \times 10^4$  to  $9.9 \times 10^5$  and  $9.1 \times 10^5$  after oxygen plasma treatment and annealing, respectively. Moreover, the rejection ratio of the annealed & plasma-treated device can reach as high as  $8.6 \times 10^6$  with a peak responsivity of  $\sim 39$  A W<sup>-1</sup>, indicating the excellent wavelength selectivity and sensitivity. The significant suppression of the visible light response of  $\beta$ -Ga<sub>2</sub>O<sub>3</sub> solar-blind photodetectors treated with annealing and oxygen plasma can be attributed to the decrease of oxygen-related vacancy defects and the surface states.

In addition, Figure 4a shows the photocurrent-time response curves of the  $\beta$ -Ga<sub>2</sub>O<sub>3</sub> photodetectors under 254 nm UV light illumination with different power densities at 10 V. All devices have excellent stability and repeatability. With increasing light power density from 0.6 to 682  $\mu$ W/cm<sup>2</sup>, the relationship between photocurrent ( $I_{\text{photo}}$ ) and power density ( $P$ ) can be well fitted using the following equation.<sup>35</sup>

$$I_{\text{photo}} = AP^\theta$$

where  $A$  is a constant and  $\theta$  is the parameter relating to the trapping and recombination process of the photo-generated electron-hole pairs in the photodetectors. By fitting the curves in Figure 4b using this equation, the  $\theta$  values of as-grown, plasma-treated, annealed, and annealed & plasma-treated  $\beta$ -Ga<sub>2</sub>O<sub>3</sub> photodetectors can be estimated to be around 0.77, 0.79, 0.81, and 0.84, respectively. The weak increase in  $\theta$  value after annealing and oxygen plasma treatment suggests the slight suppression of defect states in  $\beta$ -Ga<sub>2</sub>O<sub>3</sub>, which is in good agreement with the XPS results. Notably, the  $\theta$  value of annealed & plasma-treated  $\beta$ -Ga<sub>2</sub>O<sub>3</sub> photodetector (0.84) is still slightly lower than 1 for the ideal trap-free device, and this phenomenon may be associated with the defects in Ga<sub>2</sub>O<sub>3</sub> caused by heteroepitaxy and the defects at the electrode/semiconductor interface.

Specific detectivity ( $D^*$ ) is another important parameter to evaluate the detection ability of a photodetector. It can be calculated by

$$D^* = R / \sqrt{2qI_{\text{dark}}/S}$$

where  $R$  is the responsivity,  $q$  is the elemental charge,  $I_{\text{dark}}$  is the dark current, and  $S$  is the effective illumination area of the device.<sup>36,37</sup> In this work, the specific detectivity of the annealed & plasma-treated  $\beta$ -Ga<sub>2</sub>O<sub>3</sub> film photodetector is calculated to be  $9.0 \times 10^{15}$  cm Hz<sup>1/2</sup> W<sup>-1</sup> (Jones) owing to the high responsivity and low dark current. The performance parameters of  $\beta$ -Ga<sub>2</sub>O<sub>3</sub> MSM photodetectors at 10 V are listed in Table 1. Obviously, the annealed & plasma-treated  $\beta$ -Ga<sub>2</sub>O<sub>3</sub> MSM photodetector has the best performance among the four devices. Table 2 summarizes the performance parameters of the annealed & plasma-treated  $\beta$ -Ga<sub>2</sub>O<sub>3</sub> photodetector and the other recently reported MSM photodetectors based on Ga<sub>2</sub>O<sub>3</sub> thin films. The UV-visible rejection ratio ( $R_{\text{peak}}/R_{400}$ ) of our device is  $\sim 8.6 \times 10^6$ , which is among the highest rejection ratio reported in the literature to the best of our knowledge. What is more, the specific detectivity, the responsivity, and the dark current are comparable to or slightly better than other Ga<sub>2</sub>O<sub>3</sub> thin-film devices.

#### 4. CONCLUSIONS

In summary, we have demonstrated MSM solar-blind UV photodetectors based on  $\beta$ -Ga<sub>2</sub>O<sub>3</sub> thin films and systematically investigated the effects of annealing and/or plasma treatment on the performance of these devices. It can be found that both high-temperature oxygen annealing and oxygen plasma treatment could significantly reduce the dark current and greatly improve the UV-visible rejection ratio and NPDR. Notably, by combining the effects of high-temperature oxygen annealing and oxygen plasma treatment on the  $\beta$ -Ga<sub>2</sub>O<sub>3</sub> film, its solar-blind photodetector exhibits superior performance with a low

dark current of  $\sim 29$  pA at 10 V bias, a high NPDR of  $1.3 \times 10^{12} \text{ W}^{-1}$ , and a large rejection ratio ( $R_{\text{peak}}/R_{400}$ ) of  $8.6 \times 10^6$ . This high performance can be attributed to the reduction of the oxygen-related vacancy defects and the modification of surface states of the  $\text{Ga}_2\text{O}_3$  films after annealing and oxygen plasma treatment. Our findings suggest that the combination of high-temperature annealing and plasma treatment is an efficient way to realize high-performance  $\text{Ga}_2\text{O}_3$  film-based solar-blind UV photodetectors.

## ASSOCIATED CONTENT

### Supporting Information

The Supporting Information is available free of charge at <https://pubs.acs.org/doi/10.1021/acs.jpcc.2c07141>.

SEM images, XRD patterns, UV-visible transmission spectra,  $I$ - $V$  characteristics of different atmospheres, and treatment time in the dark (PDF)

## AUTHOR INFORMATION

### Corresponding Authors

**Kewei Liu** – State Key Laboratory of Luminescence and Applications, Changchun Institute of Optics, Fine Mechanics and Physics, Chinese Academy of Sciences, Changchun 130033, China; Center of Materials Science and Optoelectronics Engineering, University of Chinese Academy of Sciences, Beijing 100049, China; [orcid.org/0000-0001-9778-4996](https://orcid.org/0000-0001-9778-4996); Email: [liukw@ciomp.ac.cn](mailto:liukw@ciomp.ac.cn)

**Dezhen Shen** – State Key Laboratory of Luminescence and Applications, Changchun Institute of Optics, Fine Mechanics and Physics, Chinese Academy of Sciences, Changchun 130033, China; Center of Materials Science and Optoelectronics Engineering, University of Chinese Academy of Sciences, Beijing 100049, China; Email: [shendz@ciomp.ac.cn](mailto:shendz@ciomp.ac.cn)

### Authors

**Chao Zhang** – State Key Laboratory of Luminescence and Applications, Changchun Institute of Optics, Fine Mechanics and Physics, Chinese Academy of Sciences, Changchun 130033, China; Center of Materials Science and Optoelectronics Engineering, University of Chinese Academy of Sciences, Beijing 100049, China

**Qiu Ai** – State Key Laboratory of Luminescence and Applications, Changchun Institute of Optics, Fine Mechanics and Physics, Chinese Academy of Sciences, Changchun 130033, China; Center of Materials Science and Optoelectronics Engineering, University of Chinese Academy of Sciences, Beijing 100049, China

**Xiaoqian Huang** – State Key Laboratory of Luminescence and Applications, Changchun Institute of Optics, Fine Mechanics and Physics, Chinese Academy of Sciences, Changchun 130033, China; Center of Materials Science and Optoelectronics Engineering, University of Chinese Academy of Sciences, Beijing 100049, China

**Xing Chen** – State Key Laboratory of Luminescence and Applications, Changchun Institute of Optics, Fine Mechanics and Physics, Chinese Academy of Sciences, Changchun 130033, China; Center of Materials Science and Optoelectronics Engineering, University of Chinese Academy of Sciences, Beijing 100049, China

**Yongxue Zhu** – State Key Laboratory of Luminescence and Applications, Changchun Institute of Optics, Fine Mechanics

and Physics, Chinese Academy of Sciences, Changchun 130033, China; Center of Materials Science and Optoelectronics Engineering, University of Chinese Academy of Sciences, Beijing 100049, China; [orcid.org/0000-0002-5488-9541](https://orcid.org/0000-0002-5488-9541)

**Jialin Yang** – State Key Laboratory of Luminescence and Applications, Changchun Institute of Optics, Fine Mechanics and Physics, Chinese Academy of Sciences, Changchun 130033, China; Center of Materials Science and Optoelectronics Engineering, University of Chinese Academy of Sciences, Beijing 100049, China

**Zhen Cheng** – State Key Laboratory of Luminescence and Applications, Changchun Institute of Optics, Fine Mechanics and Physics, Chinese Academy of Sciences, Changchun 130033, China; Center of Materials Science and Optoelectronics Engineering, University of Chinese Academy of Sciences, Beijing 100049, China

**Binghui Li** – State Key Laboratory of Luminescence and Applications, Changchun Institute of Optics, Fine Mechanics and Physics, Chinese Academy of Sciences, Changchun 130033, China; Center of Materials Science and Optoelectronics Engineering, University of Chinese Academy of Sciences, Beijing 100049, China

**Lei Liu** – State Key Laboratory of Luminescence and Applications, Changchun Institute of Optics, Fine Mechanics and Physics, Chinese Academy of Sciences, Changchun 130033, China; Center of Materials Science and Optoelectronics Engineering, University of Chinese Academy of Sciences, Beijing 100049, China; [orcid.org/0000-0002-9714-2130](https://orcid.org/0000-0002-9714-2130)

Complete contact information is available at: <https://pubs.acs.org/10.1021/acs.jpcc.2c07141>

### Author Contributions

The manuscript was written through contributions of all authors. All authors have given approval to the final version of the manuscript.

### Notes

The authors declare no competing financial interest.

## ACKNOWLEDGMENTS

This work is supported by the National Natural Science Foundation of China (nos. 62074148, 61875194, and 11727902), the National Ten Thousand Talent Program for Young Top-notch Talents, the Key Research and Development Program of Changchun City (no. 21ZY05), the Youth Innovation Promotion Association, CAS (no. 2020225), the Jilin Province Science Fund (20220101053JC, 20210101145JC), and the Jilin Province Young and Middle-Aged Science and Technology Innovation Leaders and Team Project (20220508153RC).

## REFERENCES

- (1) Yang, J.; Liu, K.; Chen, X.; Shen, D. Recent Advances in Optoelectronic and Microelectronic Devices Based on Ultrawide-Bandgap Semiconductors. *Prog. Quant. Electron.* **2022**, *83*, 100397–100425.
- (2) Liu, K.; Sakurai, M.; Aono, M. ZnO-Based Ultraviolet Photodetectors. *Sensors* **2010**, *10*, 8604–8634.
- (3) Chen, H.; Liu, K.; Hu, L.; Al-Ghamdi, A. A.; Fang, X. New Concept Ultraviolet Photodetectors. *Mater. Today* **2015**, *18*, 493–502.

- (4) Xie, C.; Lu, X.; Tong, X.; Zhang, Z.; Liang, F.; Liang, L.; Luo, L.; Wu, Y. Recent Progress in Solar-Blind Deep-Ultraviolet Photodetectors Based on Inorganic Ultrawide Bandgap Semiconductors. *Adv. Funct. Mater.* **2019**, *29*, 1806006–1806045.
- (5) Cicek, E.; McClintock, R.; Cho, C. Y.; Rahnema, B.; Razeghi, M.  $\text{Al}_x\text{Ga}_{1-x}\text{N}$ -Based Back-Illuminated Solar-Blind Photodetectors with External Quantum Efficiency of 89%. *Appl. Phys. Lett.* **2013**, *103*, 191108–191111.
- (6) Fan, M.; Liu, K.; Chen, X.; Wang, X.; Zhang, Z.; Li, B.; Shen, D. Mechanism of Excellent Photoelectric Characteristics in Mixed-Phase  $\text{ZnMgO}$  Ultraviolet Photodetectors with Single Cutoff Wavelength. *ACS Appl. Mater. Interfaces* **2015**, *7*, 20600–20606.
- (7) Liao, M.; Koide, Y.; Alvarez, J. Photovoltaic Schottky Ultraviolet Detectors Fabricated on Boron-Doped Homoepitaxial Diamond Layer. *Appl. Phys. Lett.* **2006**, *88*, 033504–033506.
- (8) Kong, W. Y.; Wu, G. A.; Wang, K. Y.; Zhang, T. F.; Zou, Y. F.; Wang, D. D.; Luo, L. B. Graphene-Beta- $\text{Ga}_2\text{O}_3$  Heterojunction for Highly Sensitive Deep UV Photodetector Application. *Adv. Mater.* **2016**, *28*, 10725–10731.
- (9) Singh Pratiyush, A.; Krishnamoorthy, S.; Vishnu Solanke, S.; Xia, Z.; Muralidharan, R.; Rajan, S.; Nath, D. N. High Responsivity in Molecular Beam Epitaxy Grown  $\beta$ - $\text{Ga}_2\text{O}_3$  Metal Semiconductor Metal Solar Blind Deep-UV Photodetector. *Appl. Phys. Lett.* **2017**, *110*, 221107–221111.
- (10) Kaur, D.; Kumar, M. A Strategic Review on Gallium Oxide Based Deep-Ultraviolet Photodetectors: Recent Progress and Future Prospects. *Adv. Opt. Mater.* **2021**, *9*, 2002160–2002193.
- (11) Xu, J.; Zheng, W.; Huang, F. Gallium Oxide Solar-Blind Ultraviolet Photodetectors: A Review. *J. Mater. Chem. C* **2019**, *7*, 8753–8770.
- (12) Zhu, Y.; Zhang, D.; Zheng, W.; Huang, F. Multistep Thermodynamics Yielding Deep Ultraviolet Transparent Conductive  $\text{Ga}_2\text{O}_3$  Films. *J. Mater. Chem. C* **2020**, *124*, 16722–16727.
- (13) Zhang, X.; Wang, L.; Wang, X.; Chen, Y.; Shao, Q.; Wu, G.; Wang, X.; Lin, T.; Shen, H.; Wang, J.; et al. High-Performance Beta- $\text{Ga}_2\text{O}_3$  Thickness Dependent Solar Blind Photodetector. *Opt. Express* **2020**, *28*, 4169–4177.
- (14) Chen, Y.; Lu, Y.; Lin, C.; Tian, Y.; Gao, C.; Dong, L.; Shan, C. Self-Powered Diamond/Beta- $\text{Ga}_2\text{O}_3$  Photodetectors for Solar-Blind Imaging. *J. Mater. Chem. C* **2018**, *6*, 5727–5732.
- (15) Chen, X.; Ren, F.; Gu, S.; Ye, J. Review of Gallium-Oxide-Based Solar-Blind Ultraviolet Photodetectors. *Photon. Res.* **2019**, *7*, 381–415.
- (16) Li, H.; Yuan, S.-H.; Huang, T.-M.; Chen, H.-J.; Lu, F.-H.; Zhang, S.; Wu, D.-S. Impact of Thermal-Induced Sapphire Substrate Erosion on Material and Photodetector Characteristics of Sputtered  $\text{Ga}_2\text{O}_3$  Films. *J. Alloys Compd.* **2020**, *823*, 153755–153761.
- (17) Chen, X.; Liu, K.; Zhang, Z.; Wang, C.; Li, B.; Zhao, H.; Zhao, D.; Shen, D. Self-Powered Solar-Blind Photodetector with Fast Response Based on Au/ $\beta$ - $\text{Ga}_2\text{O}_3$  Nanowires Array Film Schottky Junction. *ACS Appl. Mater. Interfaces* **2016**, *8*, 4185–4191.
- (18) Guo, D.; Su, Y.; Shi, H.; Li, P.; Zhao, N.; Ye, J.; Wang, S.; Liu, A.; Chen, Z.; Li, C.; et al. Self-Powered Ultraviolet Photodetector with Superhigh Photoresponsivity (3.05 A/W) Based on the GaN/Sn: $\text{Ga}_2\text{O}_3$  pn Junction. *ACS Nano* **2018**, *12*, 12827–12835.
- (19) Lee, S. H.; Kim, S. B.; Moon, Y.; Kim, S. M.; Jung, H. J.; Seo, M. S.; Lee, K. M.; Kim, S.; Lee, S. W. High-Responsivity Deep-Ultraviolet-Selective Photodetectors Using Ultrathin Gallium Oxide Films. *ACS Photonics* **2017**, *4*, 2937–2943.
- (20) Zhao, B.; Wang, F.; Chen, H.; Zheng, L.; Su, L.; Zhao, D.; Fang, X. An Ultrahigh Responsivity (9.7 mA W<sup>-1</sup>) Self-Powered Solar-Blind Photodetector Based on Individual  $\text{ZnO}$ - $\text{Ga}_2\text{O}_3$  Heterostructures. *Adv. Funct. Mater.* **2017**, *27*, 1700264–1700271.
- (21) Dong, L.; Jia, R.; Xin, B.; Peng, B.; Zhang, Y. Effects of Oxygen Vacancies on The Structural and Optical Properties of Beta- $\text{Ga}_2\text{O}_3$ . *Sci. Rep.* **2017**, *7*, 40160–40170.
- (22) Varley, J. B.; Weber, J. R.; Janotti, A.; Van de Walle, C. G. Oxygen Vacancies and Donor Impurities in  $\beta$ - $\text{Ga}_2\text{O}_3$ . *Appl. Phys. Lett.* **2010**, *97*, 142106–142108.
- (23) Heinemann, M. D.; Berry, J.; Teeter, G.; Unold, T.; Ginley, D. Oxygen Deficiency and Sn Doping of Amorphous  $\text{Ga}_2\text{O}_3$ . *Appl. Phys. Lett.* **2016**, *108*, 022107–022110.
- (24) Zhou, C.; Liu, K.; Chen, X.; Feng, J.; Yang, J.; Zhang, Z.; Liu, L.; Xia, Y.; Shen, D. Performance Improvement of Amorphous  $\text{Ga}_2\text{O}_3$  Ultraviolet Photodetector by Annealing under Oxygen Atmosphere. *J. Alloys Compd.* **2020**, *840*, 155585–155591.
- (25) Wang, J.; Ye, L.; Wang, X.; Zhang, H.; Li, L.; Kong, C.; Li, W. High Transmittance  $\beta$ - $\text{Ga}_2\text{O}_3$  Thin Films Deposited by Magnetron Sputtering and Post-Annealing for Solar-Blind Ultraviolet Photodetector. *J. Alloys Compd.* **2019**, *803*, 9–15.
- (26) Guo, D. Y.; Wu, Z. P.; An, Y. H.; Guo, X. C.; Chu, X. L.; Sun, C. L.; Li, L. H.; Li, P. G.; Tang, W. H. Oxygen Vacancy Tuned Ohmic-Schottky Conversion for Enhanced Performance in  $\beta$ - $\text{Ga}_2\text{O}_3$  Solar-Blind Ultraviolet Photodetectors. *Appl. Phys. Lett.* **2014**, *105*, 023507–023511.
- (27) Rafique, S.; Han, L.; Zhao, H. Thermal Annealing Effect on  $\beta$ - $\text{Ga}_2\text{O}_3$  Thin Film Solar Blind Photodetector Heteroepitaxially Grown on Sapphire Substrate. *Phys. Status Solidi A* **2017**, *214*, 1700063–1700068.
- (28) Liu, M.; Kim, H. K. Ultraviolet Detection with Ultrathin  $\text{ZnO}$  Epitaxial Films Treated with Oxygen Plasma. *Appl. Phys. Lett.* **2004**, *84*, 173–175.
- (29) Zhang, Y. Y.; Qian, L. X.; Lai, P. T.; Dai, T. J.; Liu, X. Z. Improved Detectivity of Flexible a-InGaZnO UV Photodetector via Surface Fluorine Plasma Treatment. *IEEE Electron Device Lett.* **2019**, *40*, 1646–1649.
- (30) Polyakov, A. Y.; Smirnov, N. B.; Govorkov, A. V.; Baik, K. H.; Pearson, S. J.; Luo, B.; Ren, F.; Zavada, J. M. Hydrogen Plasma Passivation Effects on Properties of p-GaN. *J. Appl. Phys.* **2003**, *94*, 3960–3965.
- (31) Zhuo, Y.; Chen, Z.; Tu, W.; Ma, X.; Pei, Y.; Wang, G.  $\beta$ - $\text{Ga}_2\text{O}_3$  versus  $\epsilon$ - $\text{Ga}_2\text{O}_3$ : Control of The Crystal Phase Composition of Gallium Oxide Thin Film Prepared by Metal-Organic Chemical Vapor Deposition. *Appl. Surf. Sci.* **2017**, *420*, 802–807.
- (32) Liao, Y.; Jiao, S.; Li, S.; Wang, J.; Wang, D.; Gao, S.; Yu, Q.; Li, H. Effect of Deposition Pressure on The Structural and Optical Properties of  $\text{Ga}_2\text{O}_3$  Films Obtained by Thermal Post-Crystallization. *CrystEngComm* **2018**, *20*, 133–139.
- (33) Qian, L.; Wu, Z.; Zhang, Y.; Lai, P.; Liu, X.; Li, Y. Ultrahigh-Responsivity, Rapid-Recovery, Solar-Blind Photodetector Based on Highly Nonstoichiometric Amorphous Gallium Oxide. *ACS Photonics* **2017**, *4*, 2203–2211.
- (34) An, Y. H.; Guo, D. Y.; Li, S. Y.; Wu, Z. P.; Huang, Y. Q.; Li, P. G.; Li, L. H.; Tang, W. H. Influence of Oxygen Vacancies on The Photoresponse of  $\beta$ - $\text{Ga}_2\text{O}_3$ /SiC n–n Type Heterojunctions. *J. Phys. D: Appl. Phys.* **2016**, *49*, 285111–285116.
- (35) Zhao, Z.; Wu, D.; Guo, J.; Wu, E.; Jia, C.; Shi, Z.; Tian, Y.; Li, X.; Tian, Y. Synthesis of Large-Area 2D WS<sub>2</sub> Films and Fabrication of A Heterostructure for Self-Powered Ultraviolet Photodetection and Imaging Applications. *J. Mater. Chem. C* **2019**, *7*, 12121–12126.
- (36) Zhang, Y.; Chen, X.; Xu, Y.; Ren, F.; Gu, S.; Zhang, R.; Zheng, Y.; Ye, J. Transition of Photoconductive and Photovoltaic Operation Modes in Amorphous  $\text{Ga}_2\text{O}_3$ -Based Solar-Blind Detectors Tuned by Oxygen Vacancies. *Chin. Phys. B* **2019**, *28*, 028501–028506.
- (37) Luo, X.; Chen, S.; Liu, L.; Lv, J.; Qadir, A.; Shehzad, K.; Qiao, X.; Xu, Y.; Kienle, L.; Lotnyk, A.; et al. Solar-Blind Photodetector with High Avalanche Gains and Bias-TuMicron-Scale Photodetectors Based on One-Dimensional Single-Crystalline  $\text{Sb}_{2-x}\text{Sn}_x\text{Se}_3$  Microrods: Simultaneously Improving Responsivity and Extending Spectral Response Region. *J. Phys. Chem. C* **2018**, *123*, 810–816.
- (38) Guo, D. Y.; Zhao, X. L.; Zhi, Y. S.; Cui, W.; Huang, Y. Q.; An, Y. H.; Li, P. G.; Wu, Z. P.; Tang, W. H. Epitaxial Growth and Solar-Blind Photoelectric Properties of Corundum-Structured  $\alpha$ - $\text{Ga}_2\text{O}_3$  Thin Films. *Mater. Lett.* **2016**, *164*, 364–367.
- (39) Lee, S. H.; Lee, K. M.; Kim, Y.; Moon, Y.; Kim, S. B.; Bae, D.; Kim, T. J.; Kim, Y. D.; Kim, S.; Lee, S. W. Sub-Microsecond Response Time Deep-Ultraviolet Photodetectors Using  $\alpha$ - $\text{Ga}_2\text{O}_3$  Thin Films

Grown via Low-Temperature Atomic Layer Deposition. *J. Alloys Compd.* **2019**, *780*, 400–407.

(40) Qin, Y.; Sun, H.; Long, S.; Tompa, G. S.; Salagaj, T.; Dong, H.; He, Q.; Jian, G.; Liu, Q.; Lv, H.; et al. High-Performance Metal–Organic Chemical Vapor Deposition Grown  $\epsilon$ -Ga<sub>2</sub>O<sub>3</sub> Solar-Blind Photodetector With Asymmetric Schottky Electrodes. *IEEE Electron Device Lett.* **2019**, *40*, 1475–1478.

(41) Xu, Y.; Chen, X.; Zhou, D.; Ren, F.; Zhou, J.; Bai, S.; Lu, H.; Gu, S.; Zhang, R.; Zheng, Y.; et al. Carrier Transport and Gain Mechanisms in  $\beta$ -Ga<sub>2</sub>O<sub>3</sub>-Based Metal–Semiconductor–Metal Solar-Blind Schottky Photodetectors. *IEEE Trans. Electron Devices* **2019**, *66*, 2276–2281.

(42) Qiao, B.; Zhang, Z.; Xie, X.; Li, B.; Li, K.; Chen, X.; Zhao, H.; Liu, K.; Liu, L.; Shen, D. Avalanche Gain in Metal–Semiconductor–Metal Ga<sub>2</sub>O<sub>3</sub> Solar-Blind Photodiodes. *J. Phys. Chem. C* **2019**, *123*, 18816–18820.

(43) Xu, C.; Shen, L.; Liu, H.; Pan, X.; Ye, Z. High-Quality  $\beta$ -Ga<sub>2</sub>O<sub>3</sub> Films with Influence of Growth Temperature by Pulsed Laser Deposition for Solar-Blind Photodetectors. *J. Electron. Mater.* **2021**, *50*, 2043–2048.

(44) Yu, F.; Ou, S.; Wuu, D. Pulsed Laser Deposition of Gallium Oxide Films for High Performance Solar-Blind Photodetectors. *Opt. Mater. Express* **2015**, *5*, 1240–1249.

(45) Huang, L.; Feng, Q.; Han, G.; Li, F.; Li, X.; Fang, L.; Xing, X.; Zhang, J.; Hao, Y. Comparison Study of  $\beta$ -Ga<sub>2</sub>O<sub>3</sub> Photodetectors Grown on Sapphire at Different Oxygen Pressures. *IEEE Photonics J.* **2017**, *9*, 1–8.

(46) Liu, X.; Liu, Q.; Zhao, B.; Ren, Y.; Tao, B. W.; Zhang, W. L. Comparison of  $\beta$ -Ga<sub>2</sub>O<sub>3</sub> Thin Films Grown on r-plane and c-plane Sapphire Substrates. *Vacuum* **2020**, *178*, 109435–109440.

## □ Recommended by ACS

### Electrical Properties of HfO<sub>2</sub> on Si<sub>1-x</sub>Ge<sub>x</sub> Substrates Pretreated Using a Y Precursor with and without Subsequent Oxidant Pulsing

Woohui Lee, Hyoungsub Kim, et al.

FEBRUARY 01, 2023

ACS APPLIED ELECTRONIC MATERIALS

READ ▶

### High-Performance Diamond Phototransistor with Gate Controllable Gain and Speed

Lei Ge, Xiangang Xu, et al.

JANUARY 12, 2023

THE JOURNAL OF PHYSICAL CHEMISTRY LETTERS

READ ▶

### Engineering Strain and Texture in Ferroelectric Scandium-Doped Aluminium Nitride

Sean R. C. Mitchell, Gouri S. Kar, et al.

JANUARY 23, 2023

ACS APPLIED ELECTRONIC MATERIALS

READ ▶

### n-Type Polycrystalline Germanium Layers Formed by Impurity-Doped Solid-Phase Growth

Koki Nozawa, Kaoru Toko, et al.

JANUARY 03, 2023

ACS APPLIED ELECTRONIC MATERIALS

READ ▶

Get More Suggestions >